Journal of Petroleum Science and Technology 13(3): 39, 2023, Pages 30-42
DOI:10.22078/jpst.2024.4970.1841

Journal of Petroleum Science and Technology
Research Paper
https://jpst.ripi.ir/

Experimental and DFT Studies on the Two Imidazolium-based Ionic Liquids as Green Corrosion Inhibitors for A516-GR70 Carbon Steel in 3.5 wt.% NaCl Solution Saturated with CO_2

Ahmad Zamani, Esmaeil Akbarinezhad*, Naser Esmaeili and Jaber Neshati
Research Institute of Petroleum Industry, Tehran, Iran

Abstract
1-Dodecyl-3-methylimidazolium chloride (DDMIC) and 1-(Naphtymethyl)-3-methylimidazolium chloride (NMIC) were synthesized, and their adsorption effects on A516-Gr70 steel were investigated as a green corrosion inhibitor in 3.5 wt.% NaCl solution saturated with CO_2 at 25 °C. Potentiodynamic polarization (PDP), Scanning Kelvin probe (SKP), and electrochemical impedance spectroscopy (EIS) techniques were used to study the inhibition properties of these compounds in different concentrations. The main advantages of the two studied inhibitors, i.e., DDMIC and NMIC, are environment friendly; moreover, the inhibition performance of DDMIC is excellent, and it can reach 97% protection performance in a sweet corrosion environment. SKP studied the effects of these inhibitors on the Volta potential of the carbon steel surface. SKP analysis revealed that the trend of metal surface coverage by DDMIC can be traced via Volta's potential results. Based on SKP results, the real work function of metal surface atoms was calculated. Quantum chemical parameters of inhibitor molecules were studied by integrating density functional theory (DFT) and SKP methods. The integration results described the electron transfer mechanism during the adsorption process. Ultimately, SKP and DFT results revealed that the aromatic ring of NMIC affected its adsorption on the metal surface.

Keywords: Imidazolium, SKP, CO_2 Corrosion, Green Inhibitor, DFT (Density Functional Theory).

Introduction
Carbon dioxide is known as a corrosive species in natural gas and petroleum refining, carbon capture, and storage industries [1,2]. Carbon dioxide changes to H_2CO_3 via the hydration process in aqueous solution according to Reaction 1.

$$CO_2 + H_2O \rightleftharpoons H_2CO_3 \quad (1)$$

This acid is known as a corrosive species, and its corrosion phenomenon is named sweet corrosion [3]. Sweet corrosion has destructive effects on the metal structures of these industries and exposes them to severe problems of financial, safety, and production interruption; therefore, sweet corrosion and its control have been considered a hot topic research area for decades [3-6]. Using corrosion inhibitors is a reliable, effective, and safe solution for preventing and controlling the sweet corrosion phenomenon that takes place based on Reaction 2 [7-9].

$$Fe + H_2CO_3 \rightarrow FeCO_3 + H_2 \quad (2)$$

In order to mitigate all the risks mentioned above, investigation into the control of sweet corrosion by compounds with low negative impacts on the environment is necessary. Different corrosion inhibitors include azole derivatives such as pyrazole, bis-imidazoline, and imidazoline compounds [10-12], amidethyimidazoline [9], imidazolium [13-17] have been studied under different conditions such as temperature, flow, base metal, and CO_2 partial pressure [18-21]. The traditional inhibitors are highly toxic to humans and threaten the environment. In this context, new substances are being used, such as ionic liquids [22]. Ionic liquids can be effectively adsorbed on the metal surface, making them promising candidates to replace traditional corrosion inhibitors [23, 24].

Some azole derivatives known as ionic liquids are green inhibitors [25]. The green inhibitors prevent and control corrosion without adversely affecting health and the environment [26]. These inhibitors mitigate corrosion by adsorbing and forming film on metal surfaces. The adsorbed film changes the surface potential to positive, and a more positive surface potential results in a more noble surface. Studying surface potential helps to survey the protection mechanism and reactions on the metal surface [27]. Investigation on the adsorption of inhibitors is usually carried out via typical methods such as EIS, polarization, weight loss tests, and DFT [28-30]. Scanning Kelvin Probe (SKP) is a new non-contact method for investigating surface potential characterization, which is affected by adsorbed inhibitors [31-33]. Metal surface atoms' work function will increase

**Corresponding author:* Esmaeil Akbarinezhad, Research Institute of Petroleum Industry, Tehran, Iran
E-mail addresses: akbarinezhade@ripi.ir
Received 2024-01-20, Received in revised form 2024-02-14, Accepted 2024-03-05, Available online 2024-04-14

when surface potential increases [34]. Therefore, in this situation, the separation of electrons from iron atoms of the specimen surface by oxidation reactions will be difficult. Reduction of the oxidation process rate results in a reduced corrosion rate. Using the SKP method, the thermodynamical investigation of the electron generation power through surface atoms will be possible [35]. This method is a new approach to surveying the surface of a metal sample immersed in a solution with an inhibitor [26, 33].

Furthermore, the adsorption of inhibitor molecules on the metal surface occurs via chemical or physical processes or both. Moreover, the adsorption process is determined using the adsorption isothermal models such as Langmuir Isotherm, Freundlich Isotherm, and so on [36]. In addition, quantum chemical parameters are usually considered for studying the correlation between molecular structure and inhibitor efficiency [37,38]. It is a practical survey to determine electron interaction between inhibitor molecules and iron atoms [39].

In the present research, DDMIC and NMIC were synthesized, and their adsorption and inhibition mechanisms were investigated on A516-Gr70 steel as ionic liquids and green inhibitors in the sweet corrosion media. Moreover, the SKP method was applied to investigate inhibitor effects on the metal surface potential. Moreover, by integrating SKP and DFT as a new approach in the survey of inhibitor adsorption, the work function of specimens was obtained directly by SKP and was used to get the DFT study and analyze the parameters.

Materials and Methods

Materials

DDMIC and NMIC were synthesized (Fig. 1) and purified up to 97 (wt.%) according to reference [40]. The synthesized DDMIC and NMIC were used as green corrosion inhibitors in 25, 50, 100, 200, and 400 ppm and 25, 100, 300, and 600 ppm concentrations for A516-GR70 carbon steel in 3.5 wt.% NaCl solution saturated with CO_2. The carbon steel specimens with composition, according to Table 1, were used as a working electrode for electrochemical measurements. Specimens were prepared from A516-Gr70 steel with 10 (diameter) × 5 mm dimensions.

The samples were polished with silicon carbide abrasive paper up to 1200 grit, degreased by acetone, and dried with a nitrogen stream just before the tests. The test medium was 3.5 wt.% NaCl solution saturated with CO_2.

Methods

Electrochemical Measurements

Electrochemical impedance spectroscopy (EIS) and potentiodynamic polarization (PDP) were performed at 25 oC±1 in a three-electrode glassy cell using an Autolab-302 N potentiostat/galvanostat. The electrodes were a saturated calomel electrode (SCE), graphite rode, and carbon steel sample as reference, counter, and working electrodes.

The cell was filled with 500 ml solution, and CO_2 gas was purged into the solution for 2 hours before the working electrode was immersed in the solution. Then, CO_2 was purged into the solution continuously during electrochemical measurements. Moreover, EIS measurements started when the immersed sample's open circuit potential (OCP) reached a constant value. In addition, EIS measurements were performed in the 100 kHz to 0.01Hz frequency range and AC amplitude of 10 mV at OCP. Furthermore, PDP tests were performed immediately after the last EIS measurements. Potentiodynamic polarization tests were scanned from -250 to 250 mV versus OCP at 0.1 mV/s scan rate. The electrochemical test results were fitted using Nova1.11 version software.

Scanning Kelvin Probe

The surface Volta potential of specimens was mapped by an SKP instrument model KP Technology 5050 at 25 ±1 °C. The 768 points on the surface of specimens were scanned in an area of 15×10 mm in the central region of each specimen in X and Y directions. Tip vibration and amplitude were set at 81 Hz and 70 µm, respectively. Surface preparation and immersion conditions were performed similarly to the electrochemical tests. After immersion of specimens in the test solution, they were put in deoxygenized distill water to eliminate the NaCl effect on the specimen surface during Volta potential mapping. Then, they were dried with nitrogen gas and used in SKP measurement tests.

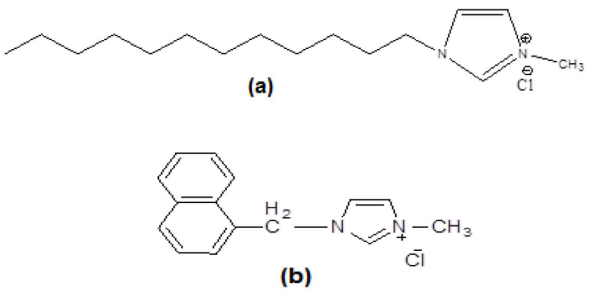

Fig. 1 molecular structures of synthesized and used ionic liquid inhibitors,(a) 1-Dodecyl-3-methylimidazolium chloride, and (b) 1-(Naphtymethyl)-3-methylimidazolium chloride

Table 1 Chemical composition of carbon steel sample

Ferrous	Silicon	Sulfur	Phosphorus	Manganese	Carbon	Elements
Balance	0.13–0.45	0.025	0.025	0.79–1.30	0.27	Composition, (wt.%)

Quantum Chemical Study

The inhibition effects of NIMC and DDMIC were studied with density functional theory (DFT) calculations. The calculations were performed using Gaussian 09 software with the DFT/B3LYP method, and 6-311G (d,p) basis set in the gaseous and aqueous phases, and DFT results were visualized using Gaussview 5. The solvent effect was studied via the Polarizable continuum model (PCM) as the default method in Gaussian 09 [41]. In this method, solvent media was distilled water by default.

Results and Discussion

Electrochemical Measurements

Electrochemical Impedance Spectroscopy

Nyquist graphs for A516-Gr70 steel immersed in the test solution with and without DDMIC and NMIC are represented in Fig. 2 and 3, respectively. Data of the Nyquist plots are modeled using electrical equivalent circuits, shown in Fig. 4, in the presence and absence of inhibitors [42].

where Rs is solution resistance, Rct is charge transfer resistance, Q_{dl} represents constant phase element, and L and Rl are inductive. Its resistance, Rinh, and Rc.p. are the resistance of inhibitor film and corrosion product, and Q_{inh} and $Q_{c.p.}$ are the constant phase elements of inhibitor film and corrosion product, respectively. A constant phase element was used in data fitting instead of a double–layer capacitor (C_{dl}) to more accurately detect the homogeneity coefficient (N) of the film [31, 32].

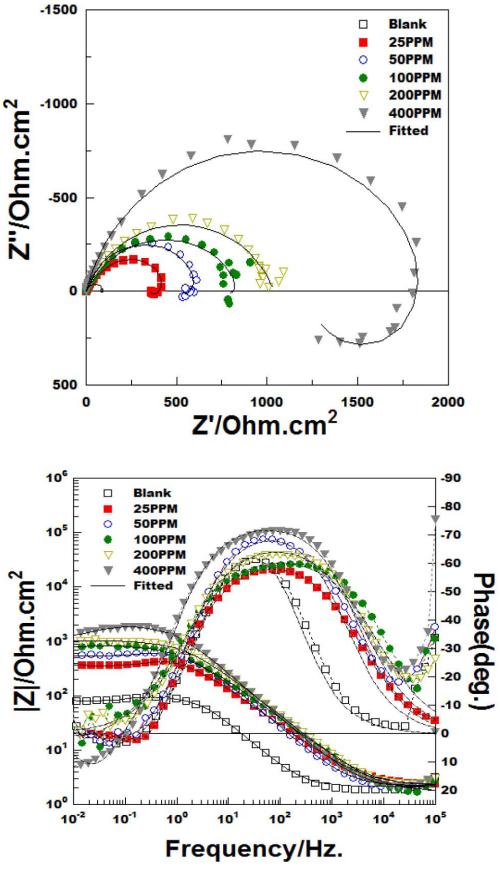

Fig. 2 Nyquist and Bode plots for A516-Gr70 in CO_2 saturated solution with 3.5 (wt.%) NaCl without and with DDMIC at 298K.

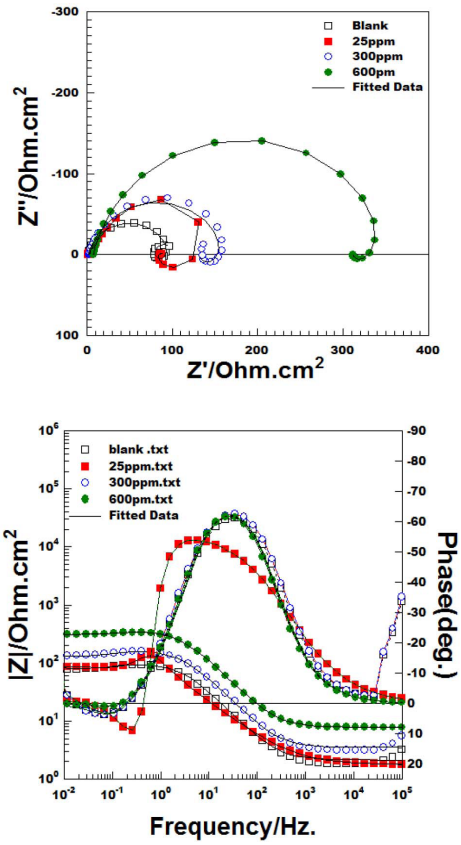

Fig. 3 Nyquist and Bode plots for A516-Gr70 in CO_2 saturated solution with 3.5 (wt.%) NaCl without and with NMIC at 298 K.

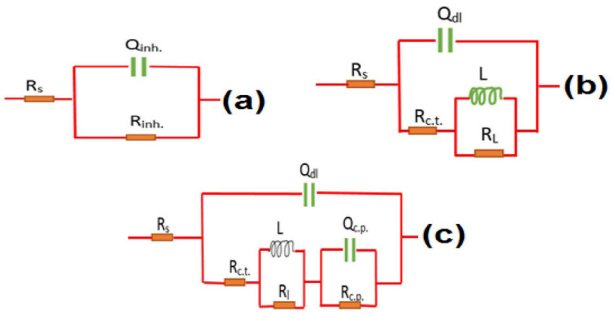

Fig. 4 Equivalent circuit model used to fit the obtained impedance spectra at 25 °C (a) with inhibitor and without inductive loop b) with inhibitor and inductive loop (c) without inhibitor.

The electrochemical impedance parameters are shown in Table 2. Based on the results of impedance elements extracted by equivalent circuits (Fig. 4), the inhibitors efficiency (θ_E) was calculated using Equation 1. Total resistance (R_T excluding R_s) is used to obtain inhibition efficiency (θ_E) [42].

$$\theta_E\,\% = \frac{R_{(inhib.)} - R_{(uninhib.)}}{R_{(inhib.)}} * 100 \qquad (3)$$

where R(inhib.) is the circuit's total resistance with an inhibitor, and R(uninhib.) is the total resistance without an inhibitor. The first semicircle of the plot in Fig. 4 is due to the constant phase element of the double layer in the blank and inhibitor solutions. The formation of iron carbide and carbonate on the specimen surface explains the second semicircle that appeared in plots of blank solution. Moreover, an inductive loop (reveres semicircle) appeared during impedance plotting at the last frequencies.

Table 2 Electrochemical impedance and inhibitor (DDMIC) efficiency parameters for A516-Gr70 in CO_2 saturated solution with 3.5 wt.% NaCl at 298 K.

Inhibitor Concentration (ppm)	R s. (Ω.cm2)	R inh. (Ω.cm2)	R c.p ($\Omega.cm_2$).	RL ($\Omega.cm_2$)	RT ($\Omega.cm_2$)	Efficiency at 300 ppm (θE)	χ^2 $\times10^{-3}$
0	2.14±0.01	77.5±1.55	23±1.15	18.5±1.14	119±2.26	--	0.4
25	2.28±0.008	315±1.014	10±0.014	15±1.18	340±0.86	65	0.1
50	0.8±0.008	620±1.48	0	0	620±0.18	81	0.2
100	1.43±0.011	854±2.19	0	0	854±3.25	86.1	0.2
200	2.08±0.016	1054±2.86	0	0	1050±4.65	89	0.7
400	11.1±0.013	1800±2.15	0	662±1.52	2462±5.78	95.2	0.4

This loop is explained by the relaxation process, which takes place by adsorbed hydrogen and ferrous hydroxide (H_{ads}, $Fe(OH)_{ads.}$) on the metal sample surface in acid media [43,44]. In this study, adsorption and the relaxation process of HCO_3^-, H_2CO_3, and Cl^- on the metal surface can cause the induction loop of the blank solution and solution with 400 ppm inhibitor. Resistance of the double layer at the specimen-solution interface increased from 80 Ω.cm^2 in blank solution to 1800 Ω.cm^2 for DDMIC in 400 ppm (94% inhibition efficiency). DDMIC forms a barrier film on the metal specimen surface by adsorption and inhibits the diffusion of aggressive species. Therefore, DDMIC performs very well in reducing CO^2 corrosion on A516-Gr70 metal. EIS plots of NMIC (Fig. 3) revealed that the efficiency of the inhibitor at maximum concentration (400 ppm) is 63%, so NMIC does not have acceptable behavior as a sweet corrosion inhibitor. In these plots, a second semicircle was made at all concentrations.

Potentiodynamic Polarization Experiments

Anodic and cathodic polarization curves of A516-Gr70 steel in a 3.5 w/v % NaCl solution saturated with CO_2 without and with different concentrations of inhibitors at 25 °C are shown in Fig. 5 and 6 for DDMIC and NMIC, respectively. Electrochemical corrosion kinetic parameters calculated by extrapolating Tafel lines and inhibitors efficiency (θ_t) were calculated by Equation 2 for inhibitors [45]. The corrosion potential (Ecorr), corrosion current density (icorr), anodic (β_a) and cathodic (β_c) Tafel slope, inhibition efficiency (θ_t), and polarization resistance (Rp) of DDMIC and NMIC are given in Tables 3 and 4.

$$\theta_t\% = \frac{i_{corr\,(uninhib.)} - i_{corr\,(inhib.)}}{i_{corr\,(uninhib.)}} * 100 \quad (4)$$

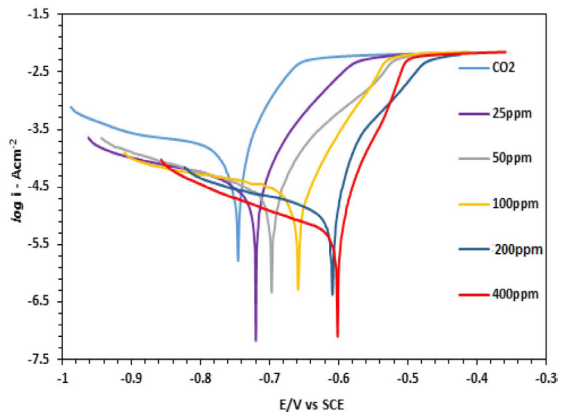

Fig. 5 Polarization curves for A516-Gr70 in CO_2 saturated solution with 3.5 (wt.%) NaCl without and with DDMIC at 298 K.

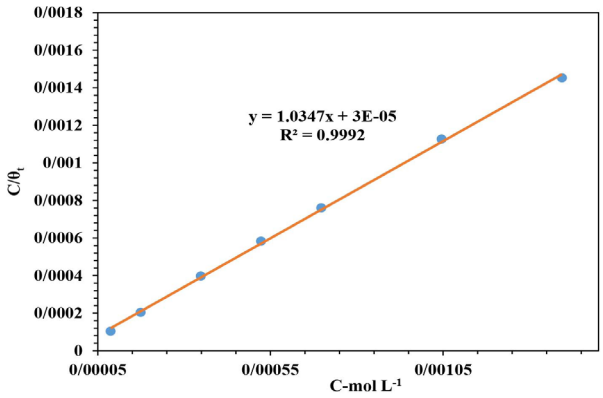

Fig. 6 Polarization curves for 516-Gr70 in CO_2 saturated solution with 3.5 (wt.%) NaCl without and with A NMIC at 298 K.

Table 3 Electrochemical parameters and inhibitor (DDMIC) efficiency for corrosion of A516-Gr70 in sweet corrosion media.

Inhibitor Concentration (ppm)	βa (V/dec)	βc (V/dec)	Ecorr (V vs. SCE)	jcorr. ×10-6 (A/cm²)	Corrosion rate (mm/year)	Polarization resistance (Ω. cm²)	Efficiency %(θt)
0	0.07	0.59	-0.76	80.3	0.94	171.5	-
25	0.19	0.05	-0.73	8.61	0.10	731.75	89
50	0.21	0.06	-0.70	7.84	0.09	941.75	90
100	0.2	0.05	-0.66	6.58	0.08	914.52	91.7
200	0.25	0.09	-0.62	4.37	0.05	2342.8	94.5
400	0.25	0.04	-0.60	1.96	0.023	2692.8	97.5

Table 4 Electrochemical parameters and inhibitor (NMIC) efficiency for corrosion of A516-Gr70 in sweet corrosion media.

Inhibitor Concentration (ppm)	β_a (V/dec)	β_c (V/dec)	Ecorr (V)	jcorr. $\times 10^{-6}$ (A/cm²)	Corrosion rate (mm/year)	Polarization resistance (Ω.cm²)	Efficiency (θ_t)
0	0.07	0.59	-0.76	80.3	0.94	171.5	-
25	0.2	0.045	-0.77	72	0.84	217.34	10
100	0.12	0.048	-0.77	60	0.70	246.91	25
300	0.14	0.044	-0.76	54	0.63	267.12	32
600	0.17	0.050	-0.73	29	0.35	568.29	63

where, $i_{corr(uninhib.)}$ and $i_{corr(inhib.)}$ are uninhibited and inhibited corrosion current densities, respectively. According to the results shown in Table 3, by adding DDMIC to the aggressive solution, corrosion potential) $E_{corr.}$ shifts positively, equal to 156 mV in final (optimum) concentration. Increasing E_{corr} enhances the nobility of the metal surface in all test concentrations. The inhibition efficiency (θ_t) of DDMIC is 96.5%. Polarization results confirmed the good performance of DDMIC on A516-Gr70 in sweet corrosion media, the same as the EIS results. Due to changes in anodic dissolution of the test metal and cathodic reduction reactions (H^+, H_2CO_3, and $HCO3^-$), β_a and β_c Tafel parameters, adsorption of DDMIC on the metal surface affects anodic and cathodic corrosion reactions, so it is a mixed type inhibitor. In order to explain the mechanism of film forming by inhibitors' molecules, the following elementary processes were proposed: (1) charged inhibitor molecules interact with charged metal by electrostatic force, (2) interaction of vacant d-orbital of Fe atoms with π electrons in imidazolium rings (3) back bonding phenomena via interaction of d orbital of Fe atoms with LUMO orbital of inhibitor molecule (4) electrostatic interaction [37, 46, 47]. In this regard, the inhibition efficiency of compounds depends on the number of adsorption active centers, consisting of interaction with the metal surface and molecular size. The adsorption of DDMIC on the metal surface occurred via the imidazolium ring (Fig. 1). The adsorption centers of DDMIC are lone pairs of N in heteroatom and π bonds of the imidazolium ring (Fig. 1). After the formation of this film, metal atoms will not be accessible for aggressive molecules in corrosive media [8, 45, 48-50].

According to polarization test results (Table 4), the corrosion inhibition efficiency of NMIC in the maximum concentration was 63%. This performance is not acceptable for a compound as a corrosion inhibitor. NMIC has a lower performance than DDMIC due to the spatial congestion of aromatic rings in the naphtymethyl group. In other words, the molecular structure affects the efficiency of NMIC [51].

Adsorption Isotherms

The adsorption mechanism of DDMIC on the A516-Gr70 steel was studied by several models based on the experimental data of the polarization technique [36]. Using the Langmuir adsorption model (Equation 3), C_{inh}/θ_t was plotted against inhibitor concentration ($C_{inh.}$) shown in Fig. 7 for the inhibitor. The correlation coefficient of the plotted line is equal to 0.9992, so the inhibitor adsorption obeys the Langmuir adsorption model excellently. Inhibitor film formed on the surface of the A516-Gr70; therefore, it is a monolayer [52]. Adsorption free energy (ΔG^0_{ads}), calculated according to Equation 4, equals -14.6 kJ/mol.

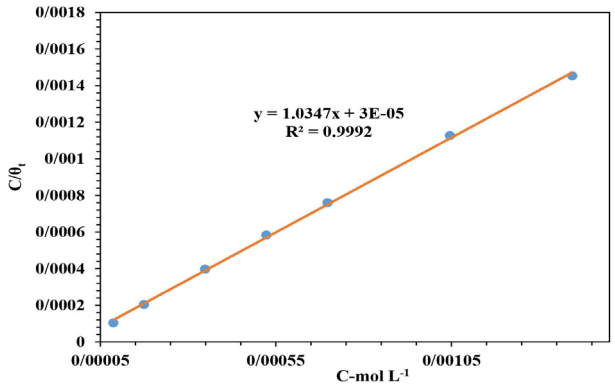

Fig. 7 Langmuir adsorption isotherm of DDMIC on A516-Gr70 in CO_2 saturated solution with 3.5 (wt.%) NaCl at 298 K.

$$\frac{C_{inh}}{\theta_t} = \alpha C_{inh} + \frac{1}{K_{ads}} \quad (5)$$

$$K_{ads} = \frac{1}{55.5} e^{\left(\frac{-\Delta G^0_{ads}}{RT}\right)} \quad (6)$$

where T is the absolute temperature (K), $C_{inh.}$ is the inhibitor concentration, R (8.314 $JK^{-1}mol^{-1}$) is the gas constant, and a is the constant. Negative values of ΔG^o_{ads} indicate that inhibitor adsorption on the metal surface is spontaneous. It is well known that values of ΔG^o_{ads} lower than -20 (kJ/mol) are ascribed to physisorption [49, 52, 53]. Hence, DDMIC is adsorbed on the metal surface through the physical process.

Scanning Kelvin Probe Measurement

The work function of surface atoms can be measured by the SKP method. Based on work function data, Volta potential (V_{CPD}) is calculated from Equation 5 [31, 54].

$$V_{CPD} = \frac{\varphi_{tip} - \varphi_{sample}}{-e} \quad (7)$$

where Φ_{sample} and Φ_{tip} are the work function of substrate and tip, respectively, and e is the electron charge. Volta potential maps of bare metal and specimens that were immersed in the blank solution and the solution containing DDMIC inhibitor at 25 °C are shown in Fig. 8a-g. Due to sweet corrosion products, the surface potential of the blank specimen increases (Fig. 8b) concerning the surface potential of the bare specimen (Fig. 8a). The surface potential of the specimens in low concentration of inhibitor (Fig. 8c) is almost as equal to surface potential of blank specimen (Fig. 8b). Increase of inhibitor concentration (Fig. 8c-g) results in higher protection of metal surface and reduction of iron carbide and carbonate as scale on specimens surface (Fig. 8). The surface potential of specimen in 400 ppm concentration of inhibitor is near to the surface potential of the bare specimen (Fig. 8g).

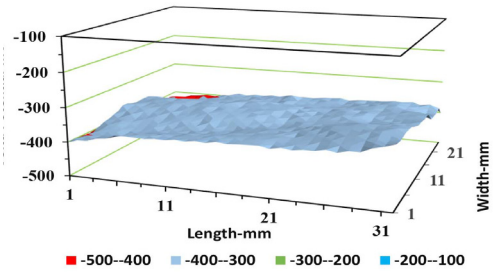

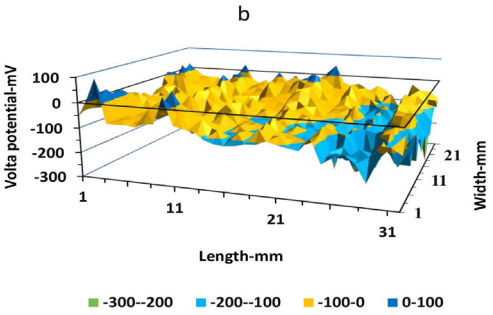

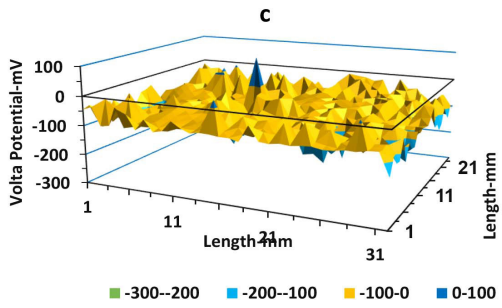

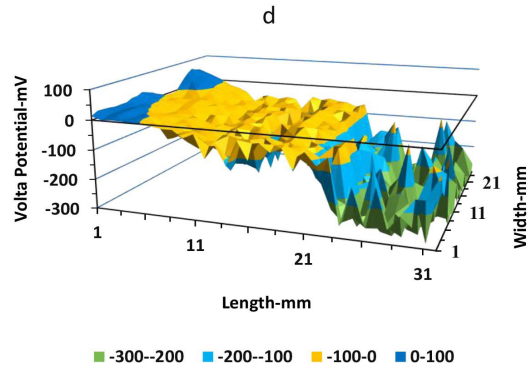

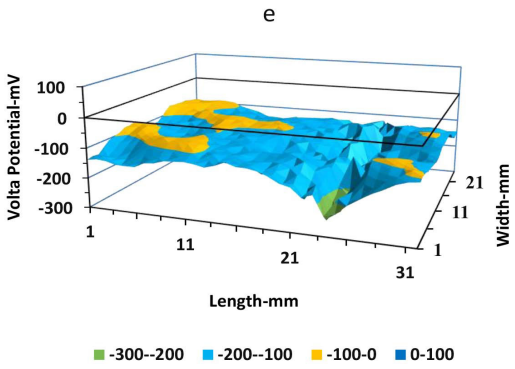

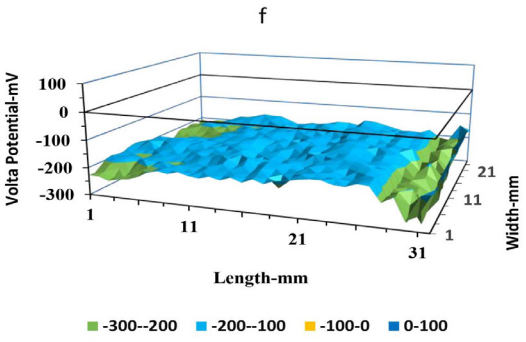

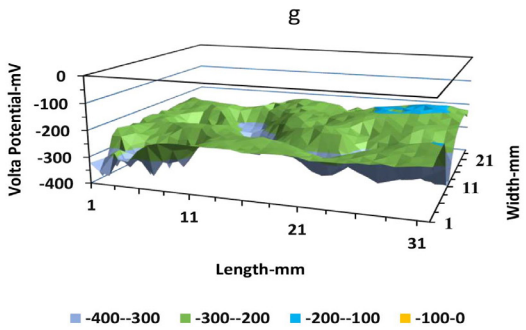

Fig. 8 Surface Volta potential mapping of A516 Gr70 (a) Bare, and exposed to CO_2 saturated solution with 3.5 (wt.%) NaCl at 298 K of DDMIC (b) 0ppm-Blank (c) 25 ppm (d) 50ppm (e) 100 ppm (f) 200ppm (g) 400 ppm.

Since DDMIC's adsorption is physical adsorption, inhibitor molecules have been removed during washing of specimen after extraction from the solution. So, most dried surfaces have the potential to be near to bare specimens. Physical condition and glossy of specimens, which shift to bare specimen surface in solution by increasing inhibitor concentration. It has almost not changed concerning the bare specimen in 400 ppm concentration of inhibitor surface potential (Fig. 8, 9, and 10).

In other words, according to Volta potential trends in Fig.10, the surface potential of specimens immersed in inhibitor solution decreases by increasing inhibitor concentration. This decrease and photographs of specimens (Fig.9) are evidence for the formation of a uniform layer on the metal surface. Therefore, the adsorption of DDMIC on the specimen surface has protected the metal. The Volta potential of a metal relates to the corrosion potential in the corrosive environment [35,55]. This relation formulated via Equation 6 is for a specimen in a solution without an inhibitor [56-58].

$$Corrosion\ potential = Cons\tan t + V_{CPD} \quad (8)$$

In this research, the solution contains an inhibitor, and according to SKP results (Fig.10), an increase in inhibitor concentration results in the reduction of the Volta potential. On the other hand, the Volta potential of immersed specimens tends to the Volta potential of bare specimens when inhibitor concentration has an increasing trend (Fig. 10). Therefore, Equation 7 can be inferred and proposed for DDMIC that was adsorbed on the A516-Gr70 steel by physical adsorption mechanism.

Inhibitor concentration increases α Corrosion potential increases α Volta potential decreases (7)

Fig. 9 Photos of specimens of A516-Gr70 exposed to CO_2 saturated solution with 3.5 %(wt.) NaCl at 298K of DDMIC after 24 hours immersion (a) 0 ppm ,Blank (b) 25 ppm (c) 50ppm (d) 100 ppm (e) 200 ppm (f) 400 ppm.

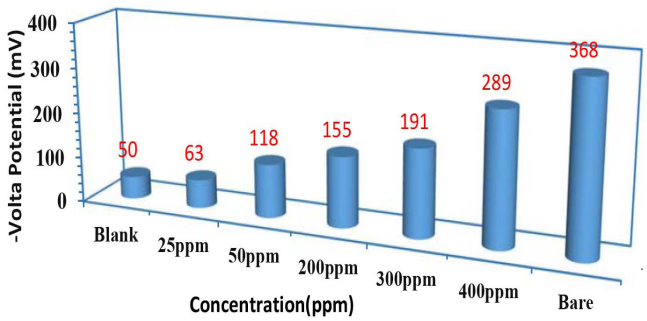

Fig. 10 Mean value of surface Volta potential of A516 Gr70; bare and exposed to CO_2 saturated solution with 3.5 %(wt.) NaCl at 298 K (with and without DDMIC.

The Volta potential of specimens in the solution with the inhibitor tends to the Volta potential of bare metal. This tendency emphasizes coverage of the specimen surface during immersion by the inhibitor. So, the trend of surface coverage can be proposed by Equation 8. Thus, based on this equation, the specimen surface coverage curve is presented in Fig. 11. This curve has a logical relation with inhibitor efficiency curves calculated by Equations 1 and 2.

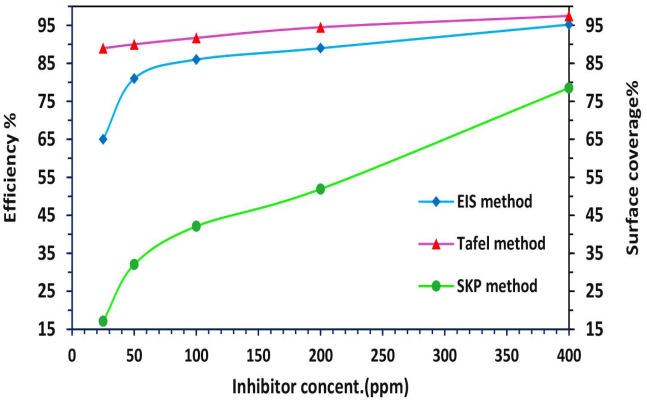

Fig. 11 Surface coverage of the A516-Gr70 steel by DDMIC

$$Metall\ Surface\ Coverage\% = (1 - \frac{V_{CPD}^{Bare} - V_{CPD}^{Inhibitor}}{V_{CPD}^{Bare}}) * 100 = \frac{V_{CPD}^{Inhibitor}}{V_{CPD}^{Bare}} * 100 \quad (8)$$

Quantum Chemical Calculation

In order to get a more comparative and theoretical survey on both inhibitors, density functional theory (DFT) and the quantum chemical parameters were used. The accurate picture of corrosive media was achieved by applying the solvent effect using a polarizable continuum model (PCM) during the simulation process. In this model, the solvent is treated as a continuum dielectric medium. The solute (inhibitor) is considered a trapped molecule in a cavity surrounded by solvent (water) [59]. Therefore, energies of frontier molecular orbitals (EHOMO, ELUMO) for the gas and water phase inhibitors were calculated using software, and the results are given in Table 5. The energy gap ΔE, the absolute electronegativity χ, the absolute chemical hardness of inhibitor η, the softness σ, the electrophilicity index $\acute{w}$, the electron transferred fraction ΔN, the difference of $LUMO_{Inh.}$ / $HOMO_{Fe}$ ($\Delta E_{(Fe\text{-}Inh.)}$), and the difference of $LUMO_{Fe}$ / $HOMO_{Inh.}$ ($\Delta E_{(Inh.\text{-}Fe)}$) are calculated by Equations 9 to 16 [17, 60, 61]. The density distribution of frontier molecular orbitals is shown in Table 6.

$$\Delta E = E_{LUMO} - E_{HOMO} \quad (9)$$

$$\chi \cong \frac{1}{2}(E_{HOMO} + E_{LUMO}) \quad (10)$$

$$\eta \cong \frac{-1}{2}(E_{HOMO} - E_{LUMO}) \quad (11)$$

$$\sigma = \frac{1}{\eta} \cong \frac{-2}{E_{HOMO} - E_{LUMO}} \quad (12)$$

$$\varpi = \frac{\chi^2}{2\eta} \quad (13)$$

$$\Delta N = \frac{\chi_{Fe} - \chi_{inh.}}{2(\eta_{Fe} + \eta_{inh.})} \quad (14)$$

$$\Delta E_{(Fe-inh.)} = LUMO_{inh.} - HOMO_{Fe} \quad (15)$$

$$\Delta E_{(inh.-Fe)} = LUMO_{Fe} - HOMO_{inh.} \quad (16)$$

Table 5 Calculated Quantum Chemical Parameters of DDMIC and NMIC.

(eV) *	(eV) *	ΔN	ẃ (eV)	Σ (eV-1)	H (eV)	X (eV)	ΔE (eV)	ELUMO (eV)	EHOMO (eV)	Inhibitor
8.92	3.86	-0.40	8.54	0.40	2.51	6.55	5.03	-4.04	-9.07	DDMIC Water phase
6.30	6.28	0.10	3.38	0.41	2.42	4.05	4.85	-1.62	-6.47	NMIC Water phase
-	-	-0.57	11.48	0.48	2.10	6.94	4.19	-4.80	-9.04	NMIC Gas phase
-	-	-0.23	6.54	0.40	2.51	5.68	5.01	-3.17	-8.18	DDMIC Gas phase

* HOMO and LUMO of Fe from [78].

Table 6 Frontier molecular orbitals density distribution of DDMIC and NMIC.

Compound	HOMO	LUMO
DDMIC	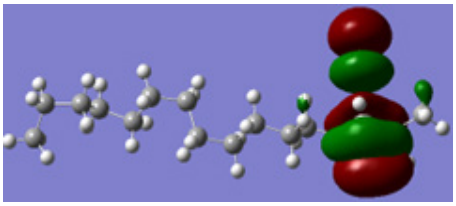	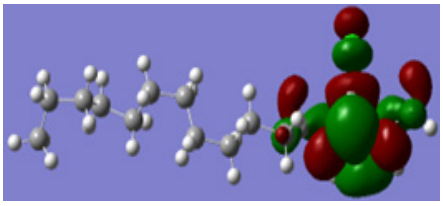
NMIC	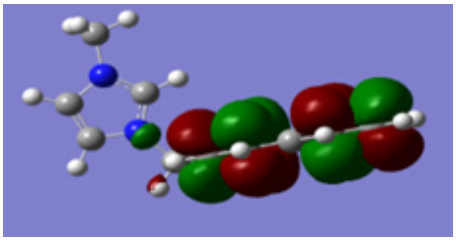	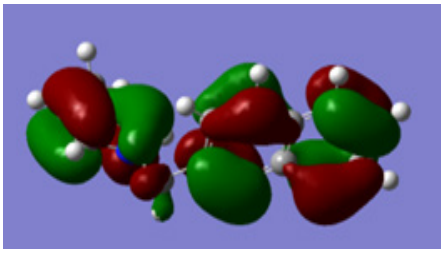

In order to include electrolyte effects on DFT calculations, the water phase results in Table 5 were considered for analysis. E_{HOMO} and E_{LUMO} are quantum chemical parameters that are associated with the electron donation ability and accepting capability, respectively. Based on the frontier molecular orbitals theory (FMO), the interaction between E_{HOMO} and E_{LUMO} affects the chemical reactivity molecule, and electron transferred fraction (ΔN) represents the mechanism of this effect. The higher value of the E_{HOMO} of the molecule is likely to indicate the tendency of a molecule to donate electrons to appropriate lower empty orbital energy (LUMO) as an acceptor [62].

To determine the electron interaction between the molecule of inhibitors and iron atoms, the electron transferred fraction (ΔN) should be calculated (Equation 14). The theoretical value of -7.0 eV for χ_{Fe} that was used in the past literature is erroneous [49]. This value corresponds to the Fermi energy of iron in the free electron gas model, where the electron-electron interaction is neglected [63, 64]. Moreover, this value was reported for metallic bulk, whereas the present research focused on the behavior of surface atoms [65]. It was shown that the work function (Φ_{Fe}) instead of electronegativity of the metal surface, it can lead to a reasonable, estimated trend of charge transfer for molecular adsorbate-metallic surface interaction. The magnitude of iron global hardness is small and negligible [47, 49]. Therefore, η_{Fe} is set to zero in Equation 14 [38], and this equation can be reported the same as recent research [66, 67]:

$$\Delta N = \frac{\phi_{Fe} - \chi_{inh.}}{2\chi_{inh.}} \quad (17)$$

The work function (Φ_{Fe}) of A516-Gr70 steel, which is needed in Equation 17, depends on the metal structure, surface preparation, microstructure planes, and position of the iron atom in the metallic crystal [64]. Because of this dependency, the different values of work function have been reported by researchers [68]. Work functions of Fe were reported for (111), (001), and (110) planes equal to 3.88, 3.91, and 4.82 eV, respectively [64,66]. In other studies, 4.5, 4.67, and 4.81eV have been considered as work functions of Fe atom in bulk, (100), and (111) planes, respectively [69, 70]. The actual value of this parameter of the metallic sample used in laboratory tests has an essential role in determining the electron transferred fraction (ΔN). In this research, as a new integrated approach, the work function of the metal specimen was measured directly using the SKP method.

For this purpose, the Volta potential of the standard sample (gold) was first mapped (Fig.12); then, using Equation 5, the work function of the probe tip was calculated. Finally, the work function of A516-Gr70 was also calculated by Equation 5 (Fig. 8a) [71]. The work function of the Fe sample obtained by this method equals -4.53eV. This value is consistent with the range mentioned in the literature for the work function of Fe [66, 69, 70]. Based on the sample's work function, the electron-transferred fraction of inhibitor adsorption was calculated using Equation 17. The ΔN amounts of DDMIC and NMIC are lower and more significant than zero, respectively. It means that the direction of the electron transfer is from iron to DDMIC and vice versa in NMIC during the adsorption process [64, 72]. In the literature, back bonding of Fe atoms has been reported as the reason for the negative sign of ΔN during adsorption. However, based on electrochemical and SKP tests, isothermal calculations, and surface facts of immersed specimens (Fig. 9), DDMIC adsorption occurs via a physical process, and there is no evidence of a chemical adsorption process. It can be concluded that DDMIC is adsorbed on Fe surface physically by van der Waals and colombic interactions or electrostatic forces [73].

Depending on the charge of the metal surface, Cl^- and N^+ in the structure of the DDMIC molecule have an essential role in the physical adsorption of DDMIC. The metal surface charge is determined by Antropov's "rational" potential of corrosion (Er), and it is calculated using the following equation (Equation 18) [74].

$$E_r = E_{ocp} - E_{pzc} \quad (18)$$

E_{ocp} and E_{pzc} are open circuit potential and potential of zero charges of the immersed specimen, respectively.

According to electrochemical tests, E_{ocp} was equal to -0.357V (SHE) in 400 ppm concentration of DDMIC. Moreover, Epzc was reported for Fe equal to -0.65 and -0.4V(SHE) for 0.3N NaCl/H_2O and 0.01N HCl/H_2O solution, respectively [75] and -0.47V(SHE) for 1M H2SO4 [76]. In the present investigation, E_{pzc} of A516-Gr70 was obtained -0.432V (SHE) in 400 ppm concentration of DDMIC by plotting polarization resistance (R_p) versus potential [74].

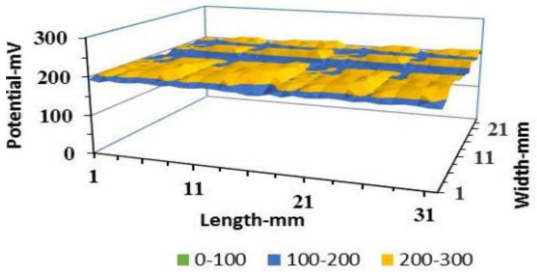

Fig. 12 Surface Volta potential mapping of gold's standard sample at 298K.

Therefore, based on Equation 18, Er will be more than zero, and the A516-Gr70 surface will be positive. It can be concluded that adsorption can occur by the polar or ionic part of the DDMIC molecule, especially Cl^- (Fig. 13) [13, 74, 77]. The molecular structure of DDMIC consists of an imidazolium ring and a long–chain hydrocarbon which are polar and hydrophobic, respectively. It is known that the hydrophobic section of a molecule is pushed back by polar molecule of water [78]. Therefore, hydrophobic part of molecule of DDMIC increases its adsorption on the metal surface [79].

Reported values of EHOMO and ELUMO for Fe are -7.9 and -0.151 eV [80, 81], and for Fe in the atomic cluster five-iron atoms, i.e., Fe5 are -5.075 and -1.747eV [67], respectively, which have been used for $\Delta E_{(Inh./Fe)}$ calculations in the water phase. According to the values of both sets, the energy difference of $LUMO_{Inh.}$ - $HOMO_{Fe}$ for DDMIC is lower than $LUMO_{Fe}$ - $HOMO_{Inh.}$ (Table 5). It means that HOMO orbital electrons of DDMIC do not tend to transfer to the LUMO orbital of iron [81]. ELUMO of DDMIC is more negative than NMIC and $\Delta E_{(Inh.-Fe)}$ of DDMIC is less than that of NMIC.

ΔN parameter is the opposite for NMIC, and it is positive. In this molecule, $\Delta E_{(Inh.-Fe)}$ is greater than $\Delta E_{(Fe-Inh.)}$. It means the π bond between NMIC's molecules and iron's atoms can be formed by electron transfer from the HOMO orbital of NMIC molecules to atoms of iron initially, and adsorption be completed finally with back donating phenomena [37, 82]. E_{HOMO} of NMIC is greater than DDMIC. It means NMIC can donate more electrons to A516-Gr70 metal than DDMIC [60]. Based on the energy gaps (ΔE) of NMIC, the naphthalene ring tends to donate more electrons to metal through the π electron cloud, but according to the result of electrochemical tests, NMIC has less adsorption on A516 Gr70 steel than DDMIC. This difference in corrosion inhibition efficiency of the inhibitor can be due to two reasons. First, the molecule of NMIC has a different part relative to DDMIC, which is a naphthalene ring. This section of the molecule causes more spatial congestion than the hydrocarbon chain in DDMIC. According to Fig. 13, the NMIC structure has a more steric hindrance effect than DDMIC (straight chain) when arranged on the metal surface by adsorption. The steric hindrance effect is a parameter affecting an inhibitor's performance [83-87]. Therefore, the molecular configuration of NMIC causes less coverage of the iron surface by the adsorption process and decreases inhibition performance. The second reason, according to results in Table 6, the HOMO energy density is highest at around the naphthalene ring. This ring consists of unsaturated bonds (double bonds). Therefore, this part of the NMIC molecule will be more polar (hydrophilic effect) than the alkane hydrocarbon straight chain of DDMIC [88]. According to the energy gap ($\Delta E_{Water\ phase}$ and $\Delta E_{Gas\ phase}$) of the inhibitors presented in Table 5, the stability increases for both inhibitors in the aqueous phase compared to the gaseous phase due to the interactions of the solvent with the inhibitor molecules. The stability energy ($\Delta E_{Water\text{-}Gas\ phase}$) of the inhibitor molecule is defined as [89, 90]:

$$\Delta E_{Water-Gas\ Phase} = E_{Water\ Phase} - E_{Gas\ Phase} \quad (19)$$

where E_{Water} phase and E_{Gas} phase are the total energy of molecules in the water and gas phase, respectively. Therefore, according to DFT output results, $\Delta E_{Water\text{-}Gas}$ phase of DDMIC and NMIC are equal to -1.9592 and -1.9390 eV, respectively. It shows that the stability of NMIC is lower than DDMIC in the water phase, and it should be adsorbed more than DDMIC on A516-Gr70. Nevertheless, experimental results showed (that) it is the reverse. This mismatch emphasizes the steric hindrance effect on NMIC adsorption.

Conclusions

The most important results of this research can be listed as follows:

1. NMIC as a corrosion inhibitor did not perform effectively on A516-GR70 steel in 3.5 wt.% NaCl solution saturated with CO_2. DDMIC affects the surface potential of immersed carbon steel and behaves as an excellent green inhibitor in the studied solution.
2. The inhibition performance of DDMIC is excellent, and it can reach 97% protection performance in a sweet corrosion environment. It obeys the Langmuir adsorption model and adsorbs on the surface of A516-GR70 steel by the physisorption mechanism. DDMIC acts as a mixed-type inhibitor by affecting anodic and cathodic reactions.
3. SKP technique was used as a powerful non-contacting

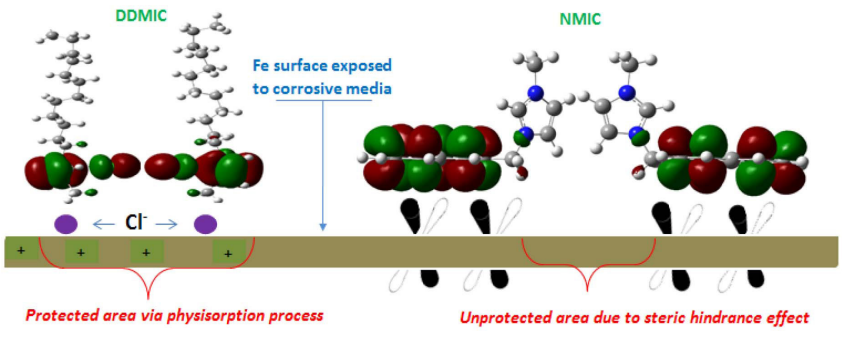

Fig. 13 Arrangement of DDMIC and NMIC molecules via adsorption process on surface of A516-Gr70 steel.

method to map the volta potential of the immersed surface and evaluate the inhibitor effect on metal surface potential.
4. The combination of DFT and SKP methods is a valuable approach for studying the adsorption effects of inhibitors on the metal surface, their adsorption mechanism, and the electron transfer process.
5. Configuration of HOMO and LUMO orbitals in molecular structure, hydrophilic/phobic effect (molecular polarity), and steric hindrance effect of DDMIC and NMIC affect adsorption process.

References

1. Kahyarian, A., Achour, M., & Nesic, S. (2017). Trends in oil and gas corrosion research and technologies, 149-190.
2. Krzemień, A., Więckol-Ryk, A., Smoliński, A., Koteras, A., & Więcław-Solny, L. (2016). Assessing the risk of corrosion in amine-based CO2 capture process, Journal of Loss Prevention in the Process Industries, 43, 189-197, doi.org/10.1016/j.jlp.2016.05.020.
3. Kahyarian, A., Singer, M., & Nesic, S. (2016). Modeling of uniform CO_2 corrosion of mild steel in gas transportation systems: a review, Journal of Natural Gas Science and Engineering, 29, 530-549, doi.org/10.1016/j.jngse.2015.12.052.
4. Wang, B., Du, M., Zhang, J., & Gao, C. J. (2011). Electrochemical and surface analysis studies on corrosion inhibition of Q235 steel by imidazoline derivative against CO_2 corrosion, Corrosion Science, 53(1), 353-361, doi.org/10.1016/j.corsci.2010.09.042.
5. Koch, G. (2017). Cost of corrosion, Trends in oil and gas corrosion research and technologies, 3-30, doi.org/10.1016/B978-0-08-101105-8.00001-2.
6. Yaro, A. S., Abdul-Khalik, K. R., & Khadom, A. A. (2015). Effect of CO2 corrosion behavior of mild steel in oilfield produced water, Journal of Loss Prevention in the Process Industries, 38, 24-38, doi.org/10.1016/j.jlp.2015.08.003.
7. Jevremović, I., Singer, M., Achour, M., Blumer, D., Baugh, T., Miskovic-Stanković, V., & Nešić, S. (2013). A novel method to mitigate the top-of-the-line corrosion in wet gas pipelines by corrosion inhibitor within a foam matrix, Corrosion, 69(2), 186-192, doi.org/10.5006/0617.
8. Chen, L., Lu, D., & Zhang, Y. (2022). Organic compounds as corrosion inhibitors for carbon steel in HCl solution: A comprehensive review, Materials, 15(6), 2023, doi.org/10.3390/ma15062023.
9. Xhanari, K., Wang, Y., Yang, Z., & Finšgar, M. (2021). A review of recent advances in the inhibition of sweet corrosion, The Chemical Record, 21(7), 1845-1875, doi.org/10.1002/tcr.202100072.
10. Farelas, F., & Ramirez, A. (2010). Carbon dioxide corrosion inhibition of carbon steels through bis-imidazoline and imidazoline compounds studied by EIS. International Journal of Electrochemical Science, 5(6), 797-814, doi.org/10.1016/S1452-3981(23)15324-7.
11. Singh, A., Ansari, K. R., Quraishi, M. A., & Kaya, S. (2020). Theoretically and experimentally exploring the corrosion inhibition of N80 steel by pyrazol derivatives in simulated acidizing environment. Journal of Molecular Structure, 1206, 127685, doi.org/10.1016/j.molstruc.2020.127685.
12. Fawzy, A., Farghaly, T. A., El-Ghamry, H. A., & Bawazeer, T. M. (2020). Investigation of the inhibition efficiencies of novel synthesized cobalt complexes of 1, 3, 4-thiadiazolethiosemicarbazone derivatives for the acidic corrosion of carbon steel, Journal of Molecular Structure, 1203, 127447, doi.org/10.1016/j.molstruc.2019.127447.
13. Zhang, Q. B., & Hua, Y. X. (2009). Corrosion inhibition of mild steel by alkylimidazolium ionic liquids in hydrochloric acid, Electrochimica Acta, 54(6), 1881-1887, doi.org/10.1016/j.electacta.2008.10.025.
14. Yang, D., Zhang, M., Zheng, J., & Castaneda, H. (2015). Corrosion inhibition of mild steel by an imidazolium ionic liquid compound: the effect of pH and surface pre-corrosion. RSC Advances, 5(115), 95160-95170, doi: 10.1039/C5RA14556B.
15. Yang, D. (2016). Corrosion inhibition performance of imidazolium ionic liquids and their influence on surface ferrous carbonate layer formation (Doctoral dissertation, University of Akron).
16. Likhanova, N. V., Domínguez-Aguilar, M. A., Olivares-Xometl, O., Nava-Entzana, N., Arce, E., & Dorantes, H. (2010). The effect of ionic liquids with imidazolium and pyridinium cations on the corrosion inhibition of mild steel in acidic environment, Corrosion Science, 52(6), 2088-2097, doi.org/10.1016/j.corsci.2010.02.030.
17. Yousefi, A., Aslanzadeh, S. A., & Akbari, J. (2018). Experimental and DFT studies of 1-methylimidazolium trinitrophenoxide as modifier for corrosion inhibition of SDS for mild steel in hydrochloric acid, Anti-Corrosion Methods and Materials, 65(1), 107-122, ISSN: 0003-5599.
18. Sim, S., Cole, I. S., Choi, Y. S., & Birbilis, N. (2014). A review of the protection strategies against internal corrosion for the safe transport of supercritical CO_2 via steel pipelines for CCS purposes, International Journal of Greenhouse Gas Control, 29, 185-199, doi.org/10.1016/j.ijggc.2014.08.010.
19. Finšgar, M., & Jackson, J. (2014). Application of corrosion inhibitors for steels in acidic media for the oil and gas industry: A review, Corrosion science, 86, 17-41, doi.org/10.1016/j.corsci.2014.04.044.
20. Cen, H., Cao, J., Chen, Z., & Guo, X. (2019). 2-Mercaptobenzothiazole as a corrosion inhibitor for carbon steel in supercritical CO_2-H_2O condition, Applied Surface Science, 476, 422-434, doi.org/10.1016/j.apsusc.2019.01.113.
21. Al-Shihry, S. S., Sayed, A. R., & Abd El-lateef, H. M. (2020). Design and assessment of a novel poly (urethane-semicarbazides) containing thiadiazoles on the backbone of the polymers as inhibitors for steel pipelines corrosion in CO_2-saturated oilfield water, Journal of Molecular Structure, 1201, 127223, doi.org/10.1016/j.molstruc.2019.127223.
22. Souza, L., Pereira, E., Matlakhova, L., Nicolin, V. A., Monteiro, S. N., & de Azevedo, A. R. (2023). Ionic liquids as corrosion inhibitors for carbon steel protection

in hydrochloric acid solution: A first review, Journal of Materials Research and Technology, 22, 2186-2205, doi.org/10.1016/j.jmrt.2022.12.066.
23. Ganjoo, R., Bharmal, A., Sharma, S., Thakur, A., Assad, H., & Kumar, A. (2022, May). Imidazolium based ionic liquids as green corrosion inhibitors against corrosion of mild steel in acidic media, In Journal of Physics: Conference Series, 2267(1), 012023, IOP Publishing, doi:10.1088/1742-6596/2267/1/012023.
24. Li, W., Tan, B., Zhang, S., Guo, L., Ji, J., Yan, M., & Wang, R. (2022). Insights into triazole derivatives as potential corrosion inhibitors in CMP process: Experimental evaluation and theoretical analysis, Applied Surface Science, 602, 154165, doi.org/10.1016/j.apsusc.2022.154165.
25. Verma, C., Ebenso, E. E., & Quraishi, M. A. (2017). Ionic liquids as green and sustainable corrosion inhibitors for metals and alloys: an overview, Journal of Molecular Liquids, 233, 403-414, doi.org/10.1016/j.molliq.2017.02.111.
26. Taghavikish, M., Dutta, N. K., & Roy Choudhury, N. (2017). Emerging corrosion inhibitors for interfacial coating, Coatings, 7(12), 217, doi.org/10.3390/coatings7120217.
27. Liu, L. & Li G. (2010). Investigation of the Surface potential on iron nanoparticles during the corrosion by atomic force microscopy (AFM)and kelvin probe force microscopy (KFM) Applied physics letters, 96: 981-993.
28. Ramachandran, S. (2017). Corrosion inhibitors—advancements in testing, Trends in Oil and Gas Corrosion Research and Technologies, 455-469, doi.org/10.1016/B978-0-08-101105-8.00019-X.
29. Popov, B. N., & Popov, B. N. (2015). Basics of corrosion measurements, Corrosion Engineering, 865, 181-237.
30. Gerengi, H. (2018). The use of dynamic electrochemical impedance spectroscopy in corrosion inhibitor studies, Protection of Metals and Physical Chemistry of Surfaces, 54, 536-540.
31. Melitz, W., Shen, J., Kummel, A. C., & Lee, S. (2011). Kelvin probe force microscopy and its application, Surface science reports, 66(1), 1-27, doi.org/10.1016/j.surfrep.2010.10.001.
32. Finot, E., Leonenko, Y., Moores, B., Eng, L., Amrein, M., & Leonenko, Z. (2010). Effect of cholesterol on electrostatics in lipid− protein films of a pulmonary surfactant, Langmuir, 26(3), 1929-1935, doi.org/10.1021/la904335m.
33. Grundmeier, G., Schmidt, W., & Stratmann, M. J. E. A. (2000). Corrosion protection by organic coatings: electrochemical mechanism and novel methods of investigation, Electrochimica Acta, 45(15-16), 2515-2533, doi.org/10.1016/S0013-4686(00)00348-0.
34. Ebrahimi, G., Rezaei, F., & Neshati, J. (2017). Investigation on corrosion protection mechanism of polyaniline nanoparticles doped with phosphoric acid by scanning Kelvin probe and other electrochemical methods, Journal of the Taiwan Institute of Chemical Engineers, 70, 427-436, doi.org/10.1016/j.jtice.2016.11.007.
35. Nazarov, A., Le Bozec, N., & Thierry, D. (2018). Scanning Kelvin Probe assessment of steel corrosion protection by marine paints containing Zn-rich primer, Progress in Organic Coatings, 125, 61-72, doi.org/10.1016/j.porgcoat.2018.08.024.
36. Ayawei, N., Ebelegi, A. N., & Wankasi, D. (2017). Modelling and interpretation of adsorption isotherms, Journal of chemistry, doi.org/10.1155/2017/3039817.
37. Gómez, B., Likhanova, N. V., Domínguez-Aguilar, M. A., Martínez-Palou, R., Vela, A., & Gazquez, J. L. (2006). Quantum chemical study of the inhibitive properties of 2-pyridyl-azoles, The Journal of Physical Chemistry B, 110(18), 8928-8934, doi.org/10.1021/jp057143y.
38. Obot, I. B., Macdonald, D. D., & Gasem, Z. M. (2015). Density functional theory (DFT) as a powerful tool for designing new organic corrosion inhibitors. Part 1: an overview, Corrosion Science, 99, 1-30, doi.org/10.1016/j.corsci.2015.01.037.
39. Gece, G. (2008). The use of quantum chemical methods in corrosion inhibitor studies, Corrosion science, 50(11), 2981-2992, doi.org/10.1016/j.corsci.2008.08.043.
40. Dzyuba, S. V., Kollar, K. D., & Sabnis, S. S. (2009). Synthesis of imidazolium room-temperature ionic liquids. Exploring green chemistry and click chemistry paradigms in undergraduate organic chemistry laboratory, Journal of chemical education, 86(7), 856, doi.org/10.1021/ed086p856.
41. M. J. Frisch, G. W. Trucks, H. B. Schlegel, G. E. Scuseria, M. A. Robb, J. R. Cheeseman, G. Scalmani, V. Barone, G. A. Petersson, H. Nakatsuji, X. Li, M. Caricato, A. Marenich, J. Bloino, B. G. Janesko, R. Gomperts, B. Mennucci, H. P. Hratchian, J. V. Ortiz, A. F. Izmaylov, J. L. Sonnenberg, D. Williams-Young, F. Ding, F. Lipparini, F. Egidi, J. Goings, B. Peng, A. Petrone, T. Henderson, D. Ranasinghe, V. G. Zakrzewski, J. Gao, N. Rega, G. Zheng, W. Liang, M. Hada, M. Ehara, K. Toyota, R. Fukuda, J. Hasegawa, M. Ishida, T. Nakajima, Y. Honda, O. Kitao, H. Nakai, T. Vreven, K. Throssell, J. A. Montgomery, Jr., J. E. Peralta, F. Ogliaro, M. Bearpark, J. J. Heyd, E. Brothers, K. N. Kudin, V. N. Staroverov, T. Keith, R. Kobayashi, J. Normand, K. Raghavachari, A. Rendell, J. C. Burant, S. S. Iyengar, J. Tomasi, M. Cossi, J. M. Millam, M. Klene, C. Adamo, R. Cammi, J. W. Ochterski, R. L. Martin, K. Morokuma, O. Farkas, J. B. Foresman, and D. J. Fox, Gaussian, Revision A. & Wallingford CT (2018). Molecular modeling and synthesis of ethyl benzyl carbamates as possible ixodicide activity, Scientific Research Publishing, 7, 1.
42. Zhang, C., Duan, H., & Zhao, J. (2016). Synergistic inhibition effect of imidazoline derivative and l-cysteine on carbon steel corrosion in a CO_2-saturated brine solution, Corrosion Science, 112, 160-169, doi.org/10.1016/j.corsci.2016.07.018.
43. Lebrini, M., Lagrenee, M., Vezin, H., Gengembre, L., & Bentiss, F. (2005). Electrochemical and quantum chemical studies of new thiadiazole derivatives adsorption on mild steel in normal hydrochloric acid medium, Corrosion Science, 47(2), 485-505, doi.org/10.1016/j.corsci.2004.06.001.
44. Zhang, G., Chen, C., Lu, M., Chai, C., & Wu, Y. (2007). Evaluation of inhibition efficiency of an imidazoline

derivative in CO_2-containing aqueous solution, Materials Chemistry and Physics, 105(2-3), 331-340, doi.org/10.1016/j.matchemphys.2007.04.076.

45. Charitha, B. P., & Rao, P. (2018). Environmentally benign green inhibitor to attenuate acid corrosion of 6061Aluminum-15%(v) SiC (P) composite, Journal of industrial and engineering chemistry, 58, 357-368, doi.org/10.1016/j.jiec.2017.09.049.
46. Alvarez, P. E., Fiori-Bimbi, M. V., Neske, A., Brandan, S. A., & Gervasi, C. A. (2018). Rollinia occidentalis extract as green corrosion inhibitor for carbon steel in HCl solution, Journal of industrial and engineering chemistry, 58, 92-99, doi.org/10.1016/j.jiec.2017.09.012.
47. El Adnani, Z., Mcharfi, M., Sfaira, M., Benzakour, M., Benjelloun, A. T., & Touhami, M. E. (2013). DFT theoretical study of 7-R-3methylquinoxalin-2 (1H)-thiones (RH; CH_3; Cl) as corrosion inhibitors in hydrochloric acid, Corrosion science, 68, 223-230, doi.org/10.1016/j.corsci.2012.11.020.
48. Arjunan, V., Balamourougane, P. S., Mythili, C. V., Mohan, S., & Nandhakumar, V. (2011). Vibrational, nuclear magnetic resonance and electronic spectra, quantum chemical investigations of 2-amino-6-fluorobenzothiazole, Journal of molecular structure, 1006(1-3), 247-258, doi.org/10.1016/j.molstruc.2011.09.015.
49. Danaee, I., Gholami, M., RashvandAvei, M., & Maddahy, M. H. (2015). Quantum chemical and experimental investigations on inhibitory behavior of amino–imino tautomeric equilibrium of 2-aminobenzothiazole on steel corrosion in H_2SO_4 solution, Journal of Industrial and Engineering Chemistry, 26, 81-94, doi.org/10.1016/j.jiec.2014.11.018.
50. Jafari, H., Akbarzade, K., & Danaee, I. (2019). Corrosion inhibition of carbon steel immersed in a 1 M HCl solution using benzothiazole derivatives, Arabian journal of chemistry, 12(7), 1387-1394, doi.org/10.1016/j.arabjc.2014.11.018.
51. Farahati, R., Behzadi, H., Mousavi-Khoshdel, S. M., & Ghaffarinejad, A. (2020). Evaluation of corrosion inhibition of 4-(pyridin-3-yl) thiazol-2-amine for copper in HCl by experimental and theoretical studies, Journal of Molecular Structure, 1205, 127658, doi.org/10.1016/j.molstruc.2019.127658.
52. Atkins, P.W. (1990) Physisorption and chemisorption in Physical Chemistry, Twelfth edittion, Oxford Univercity Press, 1-976, ISBN: 9780198847816.
53. Zhang, H. H., Gao, K., Yan, L., & Pang, X. (2017). Inhibition of the corrosion of X70 and Q235 steel in CO_2-saturated brine by imidazoline-based inhibitor. Journal of Electroanalytical Chemistry, 791, 83-94, doi.org/10.1016/j.jelechem.2017.02.046.
54. Senöz, C., Maljusch, A., Rohwerder, M., & Schuhmann, W. (2012). SECM and SKPFM Studies of the Local Corrosion Mechanism of Al Alloys–A Pathway to an Integrated SKP-SECM System, Electroanalysis, 24(2), 239-245, doi.org/10.1002/elan.201100609.
55. Nazarov, A., Le Bozec, N., & Thierry, D. (2018). Assessment of steel corrosion and deadhesion of epoxy barrier paint by scanning Kelvin probe, Progress in Organic Coatings, 114, 123-134, doi.org/10.1016/j.porgcoat.2017.09.016.
56. Stratmann, M., & Streckel, H. (1990). On the atmospheric corrosion of metals which are covered with thin electrolyte layers—I. Verification of the experimental technique, Corrosion Science, 30(6-7), 681-696, doi.org/10.1016/0010-938X(90)90032-Z.
57. Singh, A. K., & Rani, N. (2019). Scanning Kelvin probe study of steel/oil interfaces for corrosion evaluation, Materials and Corrosion, 70(7), 1162-1170, doi.org/10.1002/maco.201810577.
58. Williams, G., McMurray, H. N., & Worsley, D. A. (2002). Cerium (III) inhibition of corrosion-driven organic coating delamination studied using a scanning Kelvin probe technique. Journal of the Electrochemical Society, 149(4), B154, doi: 10.1149/1.1457983.
59. Wazzan, N. A., Al-Qurashi, O. S., & Faidallah, H. M. (2016). DFT/and TD-DFT/PCM calculations of molecular structure, spectroscopic characterization, NLO and NBO analyses of 4-(4-chlorophenyl) and 4-[4-(dimethylamino) phenyl]-2-oxo-1, 2, 5, 6-tetrahydrobenzo [h] quinoline-3-carbonitrile dyes. Journal of Molecular Liquids, 223, 29-47, doi.org/10.1016/j.molliq.2016.07.146.
60. Fergachi, O., Benhiba, F., Rbaa, M., Touir, R., Ouakki, M., Galai, M., & Touhami, M. E. (2018). Experimental and theoretical study of corrosion inhibition of mild steel in 1.0 M HCl Medium by 2 (-4 (hloro phenyl-1H-benzo [d] imidazol)-1-yl) phenyl) methanone, Materials Research, 21, e20171038, doi.org/10.1590/1980-5373-MR-2017-1038 .
61. Lv, B., Wu, K., Zhou, Z., & Jing, G. (2019). How did the corrosion inhibitor work in amino-functionalized ionic liquids for CO_2 capture: Quantum chemical calculation and experimental. International Journal of Greenhouse Gas Control, 91, 102846, doi.org/10.1016/j.ijggc.2019.102846.
62. Abd El-Lateef, H. M., Abu-Dief, A. M., & El-Gendy, B. E. D. M. (2015). Investigation of adsorption and inhibition effects of some novel anil compounds towards mild steel in H_2SO_4 solution: Electrochemical and theoretical quantum studies. Journal of Electroanalytical Chemistry, 758, 135-147, doi.org/10.1016/j.jelechem.2015.10.025.
63. Kovačević, N., & Kokalj, A. (2011). DFT study of interaction of azoles with Cu (111) and Al (111) surfaces: role of azole nitrogen atoms and dipole–dipole interactions, The Journal of Physical Chemistry C, 115(49), 24189-24197, doi.org/10.1021/jp207076w.
64. Kokalj, A. (2012). On the HSAB based estimate of charge transfer between adsorbates and metal surfaces, Chemical Physics, 393(1), 1-12, doi.org/10.1016/j.chemphys.2011.10.021.
65. Zarrouk, A., Zarrok, H., Salghi, R., Hammouti, B., Bentiss, F., Touir, R., & Bouachrine, M. O. H. A. M. M. E. D. (2013). Evaluation of N-containing organic compound as corrosion inhibitor for carbon steel in phosphoric acid, Journal Mater Environ Science, 4(2), 177-192, ISSN: 2028-2508.
66. Madkour, L. H., Kaya, S., Guo, L., & Kaya, C. (2018). Quantum chemical calculations, molecular dynamic

(MD) simulations and experimental studies of using some azo dyes as corrosion inhibitors for iron. Part 2: Bis–azo dye derivatives, Journal of Molecular Structure, 1163, 397-417, doi.org/10.1016/j.molstruc.2018.03.013.
67. Singh, A., Ansari, K. R., Chauhan, D. S., Quraishi, M. A., Lgaz, H., & Chung, I. M. (2020). Comprehensive investigation of steel corrosion inhibition at macro/micro level by ecofriendly green corrosion inhibitor in 15% HCl medium, Journal of Colloid and Interface Science, 560, 225-236, doi.org/10.1016/j.jcis.2019.10.040.
68. Riviere, J.C.(1994) Work function of simple metals: Relation between theory and experiment, First edition, Acta Physica Polonica, New York, Decker, 1-205.
69. Michaelson, H. B. (1977). The work function of the elements and its periodicity. Journal of applied physics, 48(11), 4729-4733, doi.org/10.1063/1.323539.
70. Hałas, S. (2006). 100 years of work function. Materials Science-Poland, 24(4), 951-968.
71. Ebrahimi, G., Neshati, J., & Rezaei, F. (2017). An investigation on the effect of H_3PO_4 and HCl-doped polyaniline nanoparticles on corrosion protection of carbon steel by means of scanning kelvin probe, Progress in Organic Coatings, 105, 1-8, doi.org/10.1016/j.porgcoat.2016.12.016.
72. Ma, Q., Qi, S., He, X., Tang, Y., & Lu, G. (2017). 1, 2, 3-Triazole derivatives as corrosion inhibitors for mild steel in acidic medium: Experimental and computational chemistry studies. Corrosion Science, 129, 91-101, doi.org/10.1016/j.corsci.2017.09.025.
73. Şahin, M., Gece, G., Karcı, F., & Bilgiç, S. J. J. A. E. (2008). Experimental and theoretical study of the effect of some heterocyclic compounds on the corrosion of low carbon steel in 3.5% NaCl medium, Journal of Applied Electrochemistry, 38, 809-815.
74. Yıldız, R. (2015). An electrochemical and theoretical evaluation of 4, 6-diamino-2-pyrimidinethiol as a corrosion inhibitor for mild steel in HCl solutions. Corrosion Science, 90, 544-553, doi.org/10.1016/j.corsci.2014.10.047.
75. Holze, R. (2007). Table 3.1. Electrode potentials of zero charge of metal electrodes in contact with electrolyte solutions. Electrochemical Thermodynamics and Kinetics, 223-272.
76. Popova, A., Sokolova, E., Raicheva, S., & Christov, M. (2003). AC and DC study of the temperature effect on mild steel corrosion in acid media in the presence of benzimidazole derivatives. Corrosion science, 45(1), 33-58, doi.org/10.1016/S0010-938X(02)00072-0.
77. Li, W., He, Q., Pei, C., & Hou, B. (2007). Experimental and theoretical investigation of the adsorption behaviour of new triazole derivatives as inhibitors for mild steel corrosion in acid media. Electrochimica Acta, 52(22), 6386-6394, doi.org/10.1016/j.electacta.2007.04.077.
78. Peterson, B., & Marzzacco, C. J. (2007). The effect of hydrocarbon chain length on the critical micelle concentration of cationic surfactants: An undergraduate physical chemistry experiment, Chemical Educ, 12, 80-84, doi: 10.1333/ s00897072009a, 12070080cm.
79. Manamela, K. M., Murulana, L. C., Kabanda, M. M., & Ebenso, E. E. (2014). Adsorptive and DFT studies of some imidazolium based ionic liquids as corrosion inhibitors for zinc in acidic medium, International Journal of Electrochemical Science, 9(6), 3029-3046, doi.org/10.1016/S1452-3981(23)07989-0.
80. Lide, D.R. (2007). CRC Handbook of Chemistry and Physics, 88th Edition, NY: Taylor & Francis Group.
81. Khalil, S. M., Ali-Shattle, E. E., & Ali, N. M. (2013). A theoretical study of carbohydrates as corrosion inhibitors of iron, Zeitschrift für Naturforschung A, 68(8-9), 581-586, doi: 10.5560/ZNA.2013-0037.
82. Chaitra, T. K., Mohana, K. N., Gurudatt, D. M., & Tandon, H. C. (2016). Inhibition activity of new thiazole hydrazones towards mild steel corrosion in acid media by thermodynamic, electrochemical and quantum chemical methods, Journal of the Taiwan Institute of Chemical Engineers, 67, 521-531, doi.org/10.1016/j.jtice.2016.08.013.
83. Ali, S. A., El-Shareef, A. M., Al-Ghamdi, R. F., & Saeed, M. T. (2005). The isoxazolidines: the effects of steric factor and hydrophobic chain length on the corrosion inhibition of mild steel in acidic medium, Corrosion science, 47(11), 2659-2678, doi.org/10.1016/j.corsci.2004.11.007.
84. Quraishi, M. A., Rafiquee, M. Z. A., Khan, S., & Saxena, N. (2007). Corrosion inhibition of aluminium in acid solutions by some imidazoline derivatives, Journal of Applied Electrochemistry, 37, 1153-1162.
85. Senthilkumar, A., Tharini, K., & Sethuraman, M. (2012). Steric effect of alkyl substituted piperidin-4-one oximes for corrosion control of mild steel in H_2SO_4 medium, Acta Physico-Chimica Sinica, 28(2), 399-406.
86. Bahrami Panah, N., & Danaee, I. (2019). Effect of Structural Changes on Corrosion Inhibition Behavior of Synthesized N_2O_4 Imine Compounds for Steel Pipelines in Oil and Gas Wells, Journal of Chemical and Petroleum Engineering, 53(1), 1-10, doi: 10.22059/JCHPE.2019.232647.1193.
87. Al-Sarawy, A. A., Fouda, A. S., & El-Dein, W. S. (2008). Some thiazole derivatives as corrosion inhibitors for carbon steel in acidic medium, Desalination, 229(1-3), 279-293, doi.org/10.1016/j.desal.2007.09.013.
88. Lin, I. J., Moudgil, B. M., & Somasundaran, P. (1974). Estimation of the effective number of—CH 2-groups in long-chain surface active agents, Colloid and Polymer Science, 252, 407-414.
89. Gao, J. (1996). Methods and applications of combined quantum mechanical and molecular mechanical potentials, Reviews in computational chemistry, 119-185, doi:10.1002/9780470125847.
90. Keshavarz, R. F. (2013). Theoretical study of the solvent effect on the stability energies of pyrazole and pyrazoline, Journal of Physical and Theoretical Chemistry, 9,(4), 269-273.